Electric field induced instabilities at liquid/liquid interfaces

Lin, Z. Q.; Kerle, T.; Baker, S. M.; Hoagland, D. A.; Schäffer, E.; Steiner, U.; Russell, T. P.; Schaffer, E.

Published in:
Journal of Chemical Physics

DOI:
10.1063/1.1338125

Publication date:
2001

Electric field induced instabilities at liquid/liquid interfaces

Zhiqun Lin, Tobias Kerle, Shenda M. Baker, David A. Hoagland, Erik Schäffer, Ullrich Steiner, and Thomas P. Russell

Citation: J. Chem. Phys. **114**, 2377 (2001); doi: 10.1063/1.1338125
View online: https://doi.org/10.1063/1.1338125
View Table of Contents: http://aip.scitation.org/toc/jcp/114/5
Published by the American Institute of Physics

Electric field induced instabilities at liquid/liquid interfaces

Zhiqun Lin, Tobias Kerle, Shenda M. Baker,[a] and David A. Hoagland
Department of Polymer Science and Engineering, University of Massachusetts at Amherst, Amherst, Massachusetts 01003

Erik Schäffer and Ullrich Steiner
Department of Polymer Chemistry and Materials Science Center, University of Groningen, Nijenborgh 4, 9747 AG Groningen, The Netherlands

Thomas P. Russell[b]
Department of Polymer Science and Engineering, University of Massachusetts at Amherst, Amherst, Massachusetts 01003

(Received 17 August 2000; accepted 13 November 2000)

External electric fields were used to amplify thermal fluctuations at the interface between two thin liquid films. Similar to the results shown previously for the enhancement of fluctuations at the polymer/air interface, interfacial fluctuations having a well-defined wavelength were enhanced with a characteristic growth rate. A simple theoretical framework to describe the experimental observations is presented. Both experiment and model calculation show a substantial reduction in feature size as a result of the change in surface/interfacial energy when going from the thin film to the bilayer case. Experimentally, features develop nearly 50 times faster for the bilayers in comparison to the polymer/air case. These results point to a simple route by which the nanoscopic feature can be easily and rapidly produced or replicated. © *2001 American Institute of Physics.* [DOI: 10.1063/1.1338125]

INTRODUCTION

Reorganization processes of liquids at interfaces have been studied extensively. The dynamic instabilities of thin liquid films induced by long range van der Waals interactions, i.e., spinodal dewetting,[1] for example, have been the subject of many studies theoretically[2–6] and experimentally.[7–11] Spinodal dewetting is characterized by the development of correlated fluctuations at the surface of a liquid film, ultimately leading to the disruption of the film and dewetting. In commercial applications, where film stability is crucial, this is unwanted. However, a *controlled* structure formation has potential for numerous applications. Miniaturization of these structures into the nanometer range is a desirable, albeit nontrivial, task.

A method to control structure formation at liquid/air interfaces, where electrostatic forces were used to induce an instability at the liquid/air surface of a thin film, was recently reported by Schäffer *et al.*[12,13] Their calculations indicated that the instability exhibits a well defined lateral wavelength, which follows a power-law dependence as a function of the applied electric field. Experiments[12,13] investigating thin liquid polymer films mounted between parallel capacitor plates with an air gap showed quantitative agreement between experimental data and predictions. A hexagonal array of cylinders spanning the gap between the two electrodes was found to develop. Similar observations were made by Chou and co-workers,[14,15] however, under conditions where no external electric field was applied.

Here, the findings of Schäffer *et al.*[13] are extended to the more general case of a liquid bilayer confined between two solid electrodes. Qualitatively, good agreement is found between the experimental observation and the predictions of the extended theory. More generally, the model calculations show a means by which electrically induced instabilities can be used to tune the size scale of self-assembled morphologies from the micron to the submicron level.

EXPERIMENT

Figure 1 shows the typical sample configuration used in this study. Thin liquid films of polyisoprene (PI) and oligomeric styrene (OS) were spin coated from toluene solutions onto bare and gold-coated silicon wafers, respectively. The film thickness was 140 nm. For some experiments, a small air gap was left above the liquid to form liquid/air bilayers. In the remaining experiments, the air was replaced with a layer of oligomeric dimethylsiloxane (ODMS), thus forming a liquid/liquid bilayer. No solvent was used to deposit the ODMS layer. The overall thickness of the bilayer was nominally 1 μm. Table I summarizes the physical constants of the liquid oligomers and polymers. The interfacial tension of OS/ODMS, OS/PI, and PI/ODMS are 6.1, 1.68, and 3.2 mN/m, respectively.[16] The last value was estimated from the segmental interaction parameters χ of different polymer pairs, which follow the order $\chi_{PS/PDMS} > \chi_{PI/PDMS} > \chi_{PI/PS}$.[17,18] Thin rails of silicon oxide were evaporated on top of indium–tin–oxide (ITO)-coated microscope slides (Delta Technologies), and these slides were mounted on top of the bilayer samples with the ITO and silicon oxide side facing downward, as shown in Fig. 1. The separation dis-

[a]Permanent address: Department of Chemistry, Harvey Mudd College, Claremont, CA 91711.
[b]Electronic mail: russell@mail.pse.umass.edu

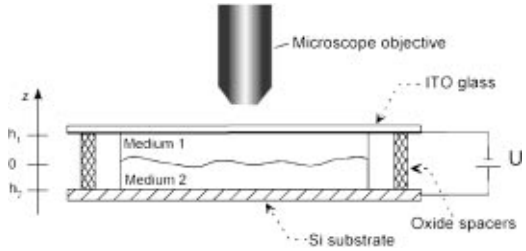

FIG. 1. Sketch of the sample geometry used in the experiments. A bilayer of two liquids is confined between two solid electrodes: a highly polished silicon wafer (lower electrode) and an ITO coated microscope slide (upper electrode). The distance between the two electrodes is controlled by the height of spacer structures (SiO) evaporated at the edges of the slides on top of the ITO. The temporal evolution of the confined samples under an applied electric field is studied by optical microscopy in the reflectance mode.

tance between the substrate (Si wafer) and the upper boundary was thus controlled by the height of the evaporated spacers and was typically 1.08 μm. The samples were placed under an optical microscope and a small voltage ($U=20$ V for PI/air, PI/ODMS bilayer experiments and $U=50$ V for OS/air, OS/ODMS bilayer experiments) was applied between the Si substrate (electrode 1) and the ITO layer (electrode 2).[19] As the ITO-coated substrates do not significantly absorb light in the visible range, this geometry permitted a direct observation of the temporal evolution of the thin liquid films in the electric field.

In the first set of experiments, a layer of PI was placed between the electrodes, leaving an air gap of 940 nm. Similar to the experiments reported recently by Schäffer *et al.*,[12] an amplification of fluctuations at the PI/air interface occurred, ultimately leading to the creation of an array of vertically standing PI columns. A typical image of this morphology can be seen in Fig. 2(a). The average distance between the center of two neighboring columns is $\langle d_{\mathrm{cyl-cyl}}\rangle = 47.4 \pm 4.4\,\mu$m.

The influence of changes in ϵ and γ of the upper layer on the time and size scales of the evolving structures was investigated in the second set of experiments. Figure 2(b) shows the final state of a PI/ODMS bilayer annealed at ambient conditions. A visual comparison of Figs. 2(a) and 2(b) shows a clear reduction in length scale, associated with the replacement of air by ODMS. The cylinder structures now exhibit a typical spacing of $\langle d_{\mathrm{cyl-cyl}}\rangle = 20.6 \pm 1.3\,\mu$m. This spacing is about one half that observed in the single film experiments. The characteristic times for the growth of the cylinders were determined for both the single and bilayers cases by optical microscopic observations. The time required to produce the first observable features was taken as the characteristic time. It is important to note that the time required to produce the cylindrical structures at the PI/ODMS interface was about 1 h, nearly 50 times faster than the time needed to produce the columns in the single film case. Additional experiments on OS/air and OS/ODMS bilayers showed essentially the same behavior, with $\langle d_{\mathrm{cyl-cyl}}\rangle = 12.7 \pm 2.8\,\mu$m for OS/air and $\langle d_{\mathrm{cyl-cyl}}\rangle = 7.6 \pm 2.9\,\mu$m of OS/ODMS.

TABLE I. The physical constants of liquid oligomers and polymer.

	OS	PI	ODMS
γ (mN/m)	39	32	20
ϵ	2.5	2.37	2.93
Mn	580	40 000	commercial grade
η (poise)	15	400	0.1

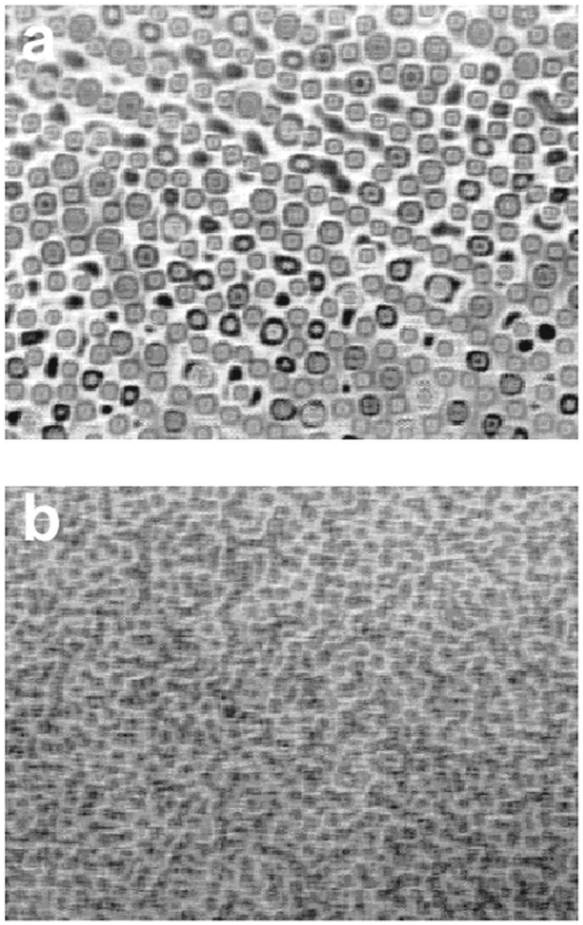

FIG. 2. (a) Optical microscopy image of a thin liquid film of polyisoprene; (b) optical microscopy image of a bilayer of polyisoprene and oligomeric dimethylsiloxane annealed for 2 days in an electric field ($h_1=940$ nm, $-h_2=140$ nm, $V=20$ V). In (a) and (b) the original color images were converted to greyscale. The dimensions of the images are 528 μm by 692 μm.

DISCUSSION

The central finding of the experiments presented is a reduction of the length scale of dynamical instabilities induced by an electric field when the liquid/air interface is replaced by a liquid/liquid interface. A reasonable starting point for the discussion of the dynamical instability is the pressure distribution along the interface itself. Similarly to the case of a thin liquid film mounted between parallel capacitor plates leaving an air gap,[12] following previous work[20–22] the overall pressure at the interface can be written as

$$p_2 = p_1 - \gamma_{12}\frac{\partial^2 \Delta h}{\partial x^2} + p_{\mathrm{el}}(\Delta h) + p_{\mathrm{dis}}(\Delta h), \tag{1}$$

where p_i is the pressure in medium i having thickness h_i; the second term is the Laplace pressure, arising from changes in

interfacial energy contribution due to changes in the interfacial area, Δh is the local displacement of interface position, p_{el} is the electrostatic pressure, and p_{dis} is the disjoining pressure. Since h_1 and h_2 are large in these studies, p_{dis} is negligible in comparison to p_{el} and the Laplace pressure and, therefore, will be neglected.[23,24]

To evaluate Eq. (1) let the origin of the coordinate system be located at the interface between the liquid layers, such that at $t=0$ the interface is located $z=0$. The system is bounded at $z=h_1$ and $z=h_2$ $(h_2<0)$. Local changes in the thickness of the layers are given by $\Delta h_1=h_1-\Delta h$ and $\Delta h_2=\Delta h-h_2$. Therefore, the electric field is given by

$$E_i=\frac{\epsilon_j U}{\epsilon_1\Delta h_2+\epsilon_2\Delta h_1} \quad (i,j=1,2;i\neq j), \tag{2}$$

where U is the applied voltage and ϵ_i is the dielectric constant of medium i. For the initial stage of the instability, when the wavelength of the instability λ is much larger than Δh, the electrostatic pressure is

$$p_{el}=-\epsilon_0(\epsilon_2-\epsilon_1)E_1E_2, \tag{3}$$

where ϵ_0 is the permittivity in a vacuum. It should be noted that this scalar approximation of the electrostatic pressure holds only for the early stages of fluctuation growth, as treated within the framework of the linear instability analysis.

Similar to the model calculations of Vrij,[25] Brochard *et al.*[3,4] and Schäffer *et al.*,[12,13] a linear stability analysis, which assumes small height fluctuations at the liquid/liquid interface of the form $\Delta h(x,t)=Be^{iqx}e^{-t/\tau}$, will yield the fastest growing mode of waves in the system. Here, q is the wave number, τ^{-1} is the growth rate, and B is the amplitude. The modulation of the interface gives rise to a pressure gradient, which induces a lateral flow J of material. The detailed flow behavior of the coupled system depends strongly on the ratio of the viscosities of the two liquids: η_1 and η_2.[22,26] The flux J can be readily obtained from $J_1=\int_{\Delta h}^{h_1}\nu_{x,1}dz$ and $J_2=\int_{h_2}^{\Delta h}\nu_{x,2}dz$ using the boundary conditions

$$\nu_{x,2}(z=h_2)=0, \quad \nu_{x,1}(z=h_1)=0, \quad \nu_{x,1}(z=0)=\nu_{x,2}(z=0)$$

and

$$\eta_1\frac{d\nu_{x,1}}{dz}_{z=\Delta h}=\eta_2\frac{d\nu_{x,2}}{dz}_{z=\Delta h},$$

where $\nu_{x,i}$ is the lateral fluid velocity in medium i. This yields

$$J_i=\frac{h_i^2}{12\eta_i(\eta_1\Delta h_2+\eta_2\Delta h_1)}\left[\eta_j\Delta h_i^2\left(-\frac{\partial p_1}{\partial x}\right)+4\eta_i\Delta h_i\Delta h_j\times\left(-\frac{\partial p_1}{\partial x}\right)+3\eta_i\Delta h_j^2\left(-\frac{\partial p_2}{\partial x}\right)\right] \quad (i,j=1,2;i\neq j). \tag{4}$$

Assuming two incompressible liquids coupled by the continuity equations

$$\frac{\partial J_1}{\partial x}+\frac{\partial J_2}{\partial x}=0, \tag{5a}$$

$$\frac{\partial\Delta h}{\partial t}+\frac{\partial(J_1-J_2)}{2\partial x}=0, \tag{5b}$$

which show the relationship of flow within the two layers, a differential equation describing the dynamic response of the interface is obtained. In the linear approximation, the dispersion relation

$$\frac{1}{\tau}=\frac{(-h_1h_2)^{3/2}}{3C(\eta)}\gamma_{12}q^4+\frac{\partial p_{el}q^2}{\partial\Delta h} \tag{6}$$

is found where $C(\eta)$ contains all terms involving viscosity, and is given by

$$C(\eta)=\frac{\eta_1^2h_2^4-\eta_1\eta_2h_1h_2(4h_1^2-6h_1h_2+4h_2^2)+\eta_2^2h_1^4}{(-h_1h_2)^{3/2}(\eta_2h_1-\eta_1h_2)}. \tag{7}$$

The fastest growing wave number, corresponding to the maximum in Eq. (6), is given by

$$q_{max}^2=\frac{\epsilon_0(\epsilon_2-\epsilon_1)^2}{\gamma_{12}U(\epsilon_1\epsilon_2)^{1/2}}(E_1E_2)^{3/2}. \tag{8a}$$

The fastest growing wavelength is found from

$$\lambda_{max}=2\pi/q_{max}=2\pi\sqrt{\frac{\gamma_{12}U(\epsilon_1\epsilon_2)^{1/2}}{\epsilon_0(\epsilon_2-\epsilon_1)^2}}(E_1E_2)^{-3/4}. \tag{8b}$$

The characteristic response time τ_{max} is then given by

$$\tau_{max}=\frac{3C(\eta)\gamma_{12}U^2\epsilon_1\epsilon_2}{(-h_1h_2)^{3/2}\epsilon_0^2(\epsilon_2-\epsilon_1)^4(E_1E_2)^3}. \tag{9}$$

Consequently, τ_{max} is proportional to γ_{12} as would be expected.[27] If we wish to compare the liquid–liquid case to the liquid–air case presented previously,[12,13] Eq. (9) can be rewritten in terms of the fastest growing wave number defined in Eq. (8a). By substitution we get

$$\tau_{max}=\frac{3C(\eta)}{\gamma_{12}(-h_1h_2)^{3/2}}q_{max}^{-4}. \tag{10}$$

In the limit of $\eta_1\ll\eta_2$, the instability is dominated by the medium with the higher viscosity. In the case where $\eta_1=0$, $\epsilon_1=1$, and $\gamma_{12}=\gamma$ (the surface tension of component 2), the equations reduce to the polymer/air case previously described by Schäffer *et al.*[12,13] The model calculations presented describe only one specific case (comparable to the experimental conditions) but it should be noted that other, more general, theoretical developments have been published by others[20,28,29] that include cylindrical bilayer configurations, gravity contributions, convection effects, and interfacial charge effects.

A comparison of experimental results to theoretical values calculated from Eq. (8b) shows qualitatively good agreement. The model calculations yield $\lambda_{max}=32.47\ \mu$m for the PI/air interface and 17.27 μm for the PI/ODMS interface, which can be compared to the experimental values of 47.4 and 20.6 μm, respectively. While experimental values are slightly higher than those predicted, both theory and experiment show a reduction of the length scale by roughly a factor of 2. Also, for the OS/air and OS/ODMS experiments, the

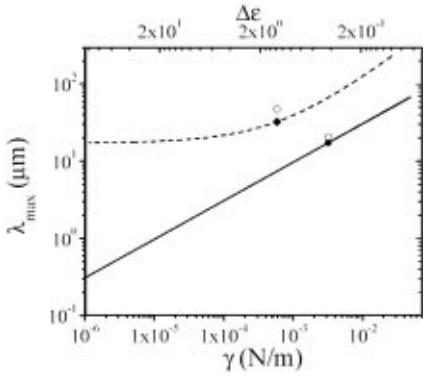

FIG. 3. Variation of the instability wavelength λ_{max} with the dielectric constant difference $\Delta\varepsilon=\varepsilon_1-\varepsilon_2$, while keeping all other parameters constant ($h_1=940$ nm, $-h_2=140$ nm, $V=20$ V, $\varepsilon_1=1$, $\gamma=32$ mN/m), as predicted by the model calculations (dashed line, left and top axis). Variation of the instability wavelength λ_{max} with γ_{12} the interfacial tension at the interface between media 1 and 2, while keeping all other parameters constant ($h_1=940$ nm, $h_2=140$ nm, $V=20$ V, $\varepsilon_1=2.93$, $\varepsilon_2=2.37$), as predicted by the model calculations (solid line, left and bottom axis). The open and solid diamonds show the measured value of $\langle d_{cyl\text{-}cyl}\rangle$ and the predicted value of λ_{max}, corresponding to Fig. 2(a) (PI single layer). The open and solid circles are $\langle d_{cyl\text{-}cyl}\rangle$ and λ_{max} corresponding to Fig. 2(b) (PI/ODMS bilayer).

model calculations and experimental values agree reasonably well, giving values of $\lambda_{max}=13.75$ and 12.94 μm, and 12.7 and 7.6 μm, respectively.

The dependence of λ_{max} on the dielectric constant difference between the liquids, i.e., $\Delta\epsilon=\epsilon_1-\epsilon_2$, while keeping other variables constant, is shown in Fig. 3 (dashed line, left and top axis). λ_{max} diverges at the point where the dielectric constants of the two media are equal, i.e., $\Delta\epsilon=0$. This is understandable since the polarizabilities of the liquids are equal and the electric field does not exert any pressure on the liquid/liquid interface. By increasing the difference between two dielectric constants, a slow decay of the preferred wavelength is observed. However, decreasing λ_{max} significantly is not possible by simply modifying the dielectric constant or increasing the applied voltage—keeping in mind that the static dielectric constants of typical materials range between 1 and 80, and that dielectric breakdown defines an upper limit for the applied voltage. The solid line (left and bottom axis) of Fig. 3 illustrates a simple route to achieve smaller sized structures. These results show the scaling of λ_{max} as a function of the interface or surface tension. It is seen that $\lambda_{max}\propto\sqrt{\gamma_{12}}$. A well-known strategy to reduce γ_{12} is by the addition of a small amount of a diblock copolymer that segregates to the liquid/liquid interface.[30–32] Similarly one can achieve an effective reduction of the surface tension of a single layer by placing a surfactant at the liquid/air interface. Studies are underway to determine the minimum achievable λ_{max} by this route.

One consequence of the reduction in λ_{max} for the bilayer is the dramatic decrease in time required to amplify fluctuations. Intuitively, one would expect that the presence of the second viscous medium would slow the growth of fluctuations substantially. On the contrary, the opposite is found. Equation (10) relates the characteristic relaxation time τ_{max} to $C(\eta)$ a term containing the viscosities, λ_{max} the characteristic wavelength, and γ_{12} the interfacial tension. Consider now $C(\eta)$ in terms of a viscosity ratio $r=\eta_1/\eta_2$. If $h=h_1=-h_2$, i.e., the layer thicknesses are equal, and $\eta_2=\eta$, then

$$C(\eta)=\eta\frac{1+14r+r^2}{1+r}. \tag{11}$$

If $r=0$, i.e., $\eta_1=0$ (thin film case) or $\eta_1\ll\eta_2$, then $C(\eta)=\eta$ and λ_{max} reduces to the result shown by Schäffer *et al.*[12,13] for a thin film with air. In the opposite extreme, $r=1$, i.e., $\eta_1=\eta_2=\eta$, then $C(\eta)=8\eta$, representing an effective eightfold increase in the viscosity. Consequently, λ_{max} would decrease by a small amount and τ_{max} should increase by a factor of 8. The observation of the 50-fold reduction in the characteristic time is in disagreement with this, as seen just by looking at Eq. (9). If we compare instabilities with the same q vector, in going from the single layer to the bilayer case, $C(\eta)$ increases and γ_{12} decreases. From Eq. (10) it is seen that this should lead to an increase of τ_{max}. For the case of (PI/ODMS), $C(\eta)$ is increased by a factor of 1.01 and γ_{12} decreases by a factor of 10, yielding a combined increase in τ of 14. Now, q increases by a factor of 1.9 or q^4 increases by a factor of 13.0. Together, these factors should cancel each other, meaning that the growth rate of the instabilities in the PI single layer and in the PI/PDMS double layers is approximately the same ($\tau_{max}=0.27$ h for the PI/air case and $\tau_{max}=0.22$ h for the PI/ODMS case). However, the time at which features are observed in the bilayers case is nearly 50 times shorter than that seen in the single layer case. The exact origin of this discrepancy is not known at present. However, the arguments presented here are valid only for the early stages of growth. Late stage processes, which govern the formation of columns (the experimental observable), require a much more detailed analysis.

CONCLUSIONS

We have extended earlier studies of field-induced structure formation in single layer liquid films to include the more general case of a bilayer. Initial experiments show, consistent with an extended model, a reduction of the characteristic length scale of fluctuations at the liquid/liquid interface. However, a marked decrease in the time constant was found in contrast to the simple model. Calculations indicate that a further decrease in the size scale is possible by a reduction of interfacial tension between the two media.

ACKNOWLEDGMENTS

This work was funded by the U.S. Department of Energy Basic Energy Sciences (T.P.R.) and Defense Programs (S.M.B.), the National Science Foundation through the Materials Research Science and Engineering Center (T.P.R.) and Division of Materials Research (S.M.B.), the Dutch ''Stichting voor Fundamenteel Onderzoek der Materie'' (U.S., E.S.), and the Deutsche Forschungsgemeinschaft (T.K.).

[1] P. Weiss, Sci. News (Washington, D. C.) **155**, 28 (1999).
[2] C. Vrij, Discuss. Faraday Soc. **42**, 23 (1967).
[3] F. Brochard-Wyart and J. Daillant, Can. J. Phys. **68**, 1084 (1990).
[4] F. Brochard-Wyart, P. Martin, and C. Redon, Langmuir **9**, 3682 (1993).

[5] E. Ruckenstein and R. K. Jain, Faraday Trans. 2 **70**, 132 (1974).
[6] A. Sharma and R. Khanna, Phys. Rev. Lett. **81**, 3463 (1998).
[7] J. Bischof, D. Scherer, S. Herminghaus, and P. Leiderer, Phys. Rev. Lett. **77**, 1536 (1996).
[8] K. Jacobs, S. Herminghaus, and K. Mecke, Langmuir **14**, 965 (1998).
[9] G. Reiter, Phys. Rev. Lett. **68**, 75 (1992).
[10] T. Kerle, R. Yerushalmi-Rozen, J. Klein, and L. J. Fetters, Europhys. Lett. **44**, 484 (1998).
[11] R. Xie, A. Karim, J. F. Douglas, C. C. Han, and R. A. Weiss, Phys. Rev. Lett. **81**, 1251 (1998).
[12] E. Schäffer, T. Thurn-Albrecht, T. P. Russell, and U. Steiner, Nature (London) **403**, 874 (2000).
[13] E. Schäffer, T. Thurn-Albrecht, T. P. Russell, and U. Steiner, Europhys. Lett. (in press).
[14] S. Y. Chou, L. Zhuang, and L. Guo, Appl. Phys. Lett. **75**, 1004 (1999).
[15] S. Y. Chou and L. Zhuang, J. Vac. Sci. Technol. B **17**, 3197 (1999).
[16] S. Wu, *Polymer Interface and Adhesion* (Marcel Dekker, New York, 1982).
[17] E. Helfand and Y. Tagami, J. Chem. Phys. **56**, 3592 (1972).
[18] E. Helfand and Z. R. Wasserman, Macromolecules **9**, 879 (1976).
[19] We independently determined the resistivity of the ITO layer ($R_{\mathrm{ITO}} = 320\,\Omega$) and the resistivity of the highly doped Si wafers ($R_{\mathrm{Si}} = 0.01-0.03\,\Omega/\mathrm{cm}$). Considering the typical currents measured during the experiment $I \approx 5\,\mu$A this indicates that the applied potential indeed dropped over the sample capacitor.
[20] A. Onuki, Physica A **217**, 38 (1995).
[21] U. Killat, J. Appl. Phys. **46**, 5169 (1975).
[22] G. K. Batchelor, *An Introduction to Fluid Dynamics* (Cambridge University Press, Cambridge, 1967).
[23] B. V. Derjaguin, N. V. Churaev, and V. M. Muller, *Surface Forces* (Consultants Bureau, New York, 1987).
[24] J. N. Israelachvili, *Intermolecular and Surface Forces*, 2nd ed. (Academic, London, 1992).
[25] A. Vrij, Discuss. Faraday Soc. **42**, 23 (1966).
[26] C. W. Macosko, *Rheology Principles, Measurements and Applications* (Wiley, New York, 1994).
[27] G. Reiter, R. Khanna, and A. Sharma, Phys. Rev. Lett. **85**, 1432 (2000).
[28] J. M. Reynolds, Phys. Fluids **8**, 161 (1965).
[29] J. R. Melcher and C. V. Smith, Phys. Fluids **12**, 778 (1969).
[30] J. Kohler, G. Riess, and A. Banderet, Eur. Polym. J. **4**, 173 (1968); **4**, 187 (1968).
[31] S. H. Anastasiadis, I. Gancarz, and J. T. Koberstein, Macromolecules **22**, 1449 (1989).
[32] A. Budkowski, J. Klein, U. Steiner, and L. J. Fetters, Macromolecules **26**, 2470 (1993).